Binary Black Hole Coalescence

Alessandra Buonanno

Citation: AIP Conference Proceedings **968**, 307 (2008); doi: 10.1063/1.2840417
View online: http://dx.doi.org/10.1063/1.2840417
View Table of Contents: http://scitation.aip.org/content/aip/proceeding/aipcp/968?ver=pdfcov
Published by the AIP Publishing

Binary Black Hole Coalescence

Alessandra Buonanno

Maryland Center for Fundamental Physics, Department of Physics, University of Maryland, College Park, MD 20742

Abstract. Recent work at the interface between analytical and numerical relativity is deepening our understanding of the two-body dynamics and of the gravitational radiation from binary black-hole coalescences. In this talk we review the most recent advances, focusing on the transitions from inspiral to merger and to ringdown, and on the recoil velocity of the newly born black hole.

INTRODUCTION

A number of recent developments in numerical relativity have allowed for stable evolution of binary black hole coalescence. After the initial breakthroughs [1, 2, 3], several numerical-relativity groups have built reliable codes and produced more and more accurate simulations, exploring larger regions of the parameter space [4, 5, 6, 7, 9] Along these impressive results, the analytical interface of the numerical simulations is also deepening our understanding of the two-body dynamics and gravitational radiation. In particular, the studying of the transition inspiral to merger to ringdown has revealed an intriguing *simplicity*. This is certainly true for non-spinning comparable-mass binaries moving along quasi-circular orbits [10, 11], and for a test-mass plunging in a Schwarzschild black hole [12]. By combining the post-Newtonian [13], close-limit-approximation [14] and test-mass-limit predictions, [15, 16] this simplicity was anticipated by the analytical effective-one-body model [17, 18, 19, 20, 21] and the numerical Lazarus project [22]. As we shall review, after a long, adiabatic inspiral, the *two-body* crosses a rather blurred last stable circular orbit, travels along a still adiabatic plunge, and, finally, as the dominant gravitational-wave frequency rises *rapidly*, exciting by resonance the ringdown modes, *one-body*, a quasi-stationary Kerr black hole, is left behind. It turns out that the direct gravitational radiation from the two black holes is strongly filtered by the curvature potential once the two black holes are inside it. As a consequence, the part of the energy produced in the strong-burst of $\sim 10-15M$, between the end of the inspiral(-plunge) and the beginning of the ringdown, seems to be momentarily *stored in the resonant cavity of the geometry, inside the curvature potential, and then slowly released in ringdown modes* [16].

Another relevant research topic at the interface between analytical and numerical techniques, has been the computation of the recoil velocity (or *kick*) of merging black holes. The kick is due to *beamed* emission of gravitational-wave radiation [23, 24, 25]. The magnitude of the kick is particularly interesting in astrophysics for understanding the growth of supermassive black holes, which exist at the center of most galaxies. How the recoil distribution depends on the black hole mass ratio and spins affects the hierarchical structure formation of the host galaxies [26, 27].

CP968, *Astrophysics of Compact Objects, International Conference on Astrophysics of Compact Objects*
edited by Y.-F. Yuan, X.-D. Li, and D. Lai

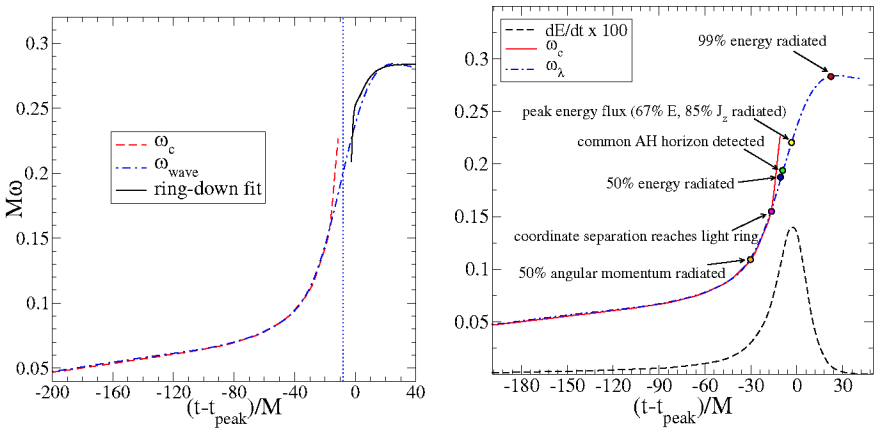

FIGURE 1. In the left panel we plot the dominant frequencies evaluated from the orbit, ω_c (short dashed red line), and from the wave, ω_λ (the dot-dashed blue line). The thick solid (black) line shows the dominant frequency as fit to the ringdown signal. The vertical dotted (blue) line marks the approximate time that a common apparent horizon forms. In the right panel we show some features of the merger phase for an equal-mass binary as discussed in Ref. [10]. (Both figures are adapted from Ref. [10].)

Gravitational radiation from merging black holes

The network of ground-based laser-interferometer gravitational-wave detectors, such as LIGO [28], Virgo [29], GEO [30] and TAMA [31], are currently operating at design sensitivity (except for Virgo which is expected to reach design sensitivity by the end of the year) and are searching for gravitational waves in the frequency range of 10–10^3 Hz. Within the next decade those detectors will likely be complemented by the laser-interferometer space antenna (LISA) [32], a joint venture between NASA and ESA, which will search for gravitational waves in the frequency range 3×10^{-5}–10^{-1} Hz.

The search for gravitational waves from coalescing binary systems and the extraction of parameters are based on the matched-filtering technique [33], which requires accurate knowledge of the waveform of the incoming signal. The best-developed *analytical* method for describing the two-body dynamics and the gravitational-wave signal during the long inspiral phase is undoubtedly the post-Newtonian (PN) expansion [13]. For compact bodies the latter is essentially an expansion in the characteristic orbital velocity v/c. Predictions for the gravitational-wave phasing are currently available through 3.5PN order [13] (v^7/c^7), if the compact objects do not carry spin, and 2.5PN order [13] (v^5/c^5) if they carry spin. Resummation of the post-Newtonian expansion aimed at pushing analytical calculations until the final stage of evolution, including the transition inspiral to merger to ringdown, have been worked out, notably the effective-one-body approach [21, 17, 18, 19, 35, 36, 37] which maps the two-body problem to the dynamics of a test-particle in a suitably defined spacetime.

After the two black holes merge, the system settles down to a Kerr black hole and emits quasi-normal modes (QNMs) [34, 15]. This phase is commonly known as the ringdown (RD) phase. Since the QNMs have complex frequencies totally determined by

the black-hole's mass and spin, the RD waveform is a superposition of damped sinusoidals. Thus, the inspiral and ringdown waveforms can be computed analytically. What about the merger? Since the nonlinearities dominate, the merger would be described at *best* and *utterly* through numerical simulations of Einstein equations. However, before the numerical-relativity results became a reality, some analytical approaches were proposed. In the test-mass limit, Refs. [16, 15] realized a long time ago that the basic physical reason underlying the presence of a universal merger signal was that when a test particle falls below $3M$ (the unstable light storage ring of Schwarzschild), the gravitational-wave it generates is strongly filtered by the curvature potential barrier centered around it. For the equal-mass case, Ref. [14] proposed the so-called close-limit approximation, which consists in switching from the two-body description to the one-body description (perturbed-black-hole) close to the light-ring location. Based on these observations, the EOB resummation scheme [17, 18, 19, 35, 36] provided a first *example* of full waveform by (i) resumming the PN Hamiltonian, (ii) modeling the merger as a very short (instantaneous) phase and (iii) matching the end of the plunge (around the light-ring) with the RD phase (see Ref. [22] where similar ideas were developed also in numerical relativity). The matching was initially done using *only* the least damped QNM whose mass and spin were determined by the binary black-hole energy and angular momentum at the end of the plunge. Today, with the spectacular results in numerical-relativity, we are in the position of assessing the closeness of analytical to numerical waveforms for inspiral, merger and ringdown.

Quite interestingly, numerical simulations are showing that the merger accounts for only a brief time ($\sim$ 10–15M) compared to the inspiral (arbitrarily long) or ringdown phases, as can be seen in Fig. 1. In the left panel we plot the frequency computed in Pretorius numerical simulation [10] and evaluated from the orbit, from the wave, and from a ringdown fit. The frequencies from the orbit and the wave decouple about $20M$ before the peak in the waveform, indicating that close to the common apparent horizon formation the gravitational-wave emission is no-longer driven by the orbital motion but by the ringing of spacetime through the production of ringdown modes. The latter are excited by the fast rise of the frequency. In the right panel we show the frequency evaluated from the wave and the gravitational-wave energy flux (multiplied by 100) for an equal-mass binary. We mark with circles several relevant events [10]. Notably, the time when the common apparent horizon of the final black hole first appears, when the binary separation reaches the light-ring of the final black hole, the peak of the radiation flux (which occurs around $3-4M$ before the peak in the amplitude of the waveform), when 50% of the energy and angular momentum have been radiated, and the time when 99% of the energy has been radiated. Although the merger is quite short, the dominant gravitational-wave frequency rises very quickly and spans a significant range of frequencies during this phase. With current data, the peak in the waveform seems to be a natural point to mark the transition between the merger and ringdown phases. It is quite possible that the higher-order ringdown modes/overtones are excited by resonance with the dominant gravitational-wave frequency as it rises during the merger.

Figure 2 shows the comparison between the numerical relativity and the EOB model in the equal-mass case, as obtained in Ref. [11]. Similar results were also obtained in the case of mass ratios $4:1{,}2:1{,}3:2$. However, Ref. [11] cannot draw definite conclusions about the EOB model's inspiral performance because the results depend on

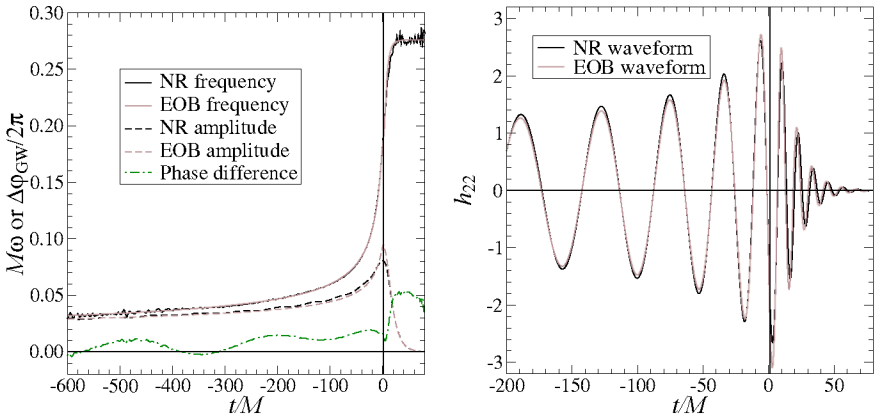

FIGURE 2. Comparison between inspiral-merger-ringdown frequency (left panel) and waveform (right panel) for a non-spinning equal-mass black-hole binary, as predicted by the EOB model [19, 18, 10, 11] and as obtained in the numerical simulation by Goddard/NASA. (Both figures are adapted from Ref. [11].)

the mass ratios, and extremely accurate, long-lasting numerical-relativity simulations are not available, yet, for unequal masses. Therefore, we do not exclude other possible adjustments in the EOB model to keep track of the phase evolution for an extremely large number of gravitational-wave cycles.

Those comparisons are suggesting that it should be possible to design purely analytical templates with the full numerics used to guide the patching together of the inspiral and RD waveforms. This is an important avenue to template construction as eventually hundreds of thousands of waveform templates may be needed to extract the signal from the noise, an impossible demand for numerical-relativity alone.

Recoil velocity from merging black holes

Gravitational waves carry away from the binary both energy and angular-momentum. Due to some asymmetry in the binary system [23, 24, 25], such as unequal masses and/or spins of different magnitude and orientation, gravitational-waves can carry away also a net linear momentum. Because of linear-momentum conservation, the black hole that forms after merger acquires a recoil velocity or kick. The recoil velocity has astrophysical importance because it can affect the growth of supermassive black holes, through hierarchical mergers [26, 27]. In those scenarios dark-matter halos grow through hierarchical mergers. The supermassive black holes at the centers of such haloes inevitably merge unless they are kicked out of the gravitational-potential well because the recoil velocity gained in a previous merger is larger than the halo's escape velocity. Recently, both in the analytical and numerical relativity communities a great deal of effort has been directed towards the computation of the recoil velocity of the final black hole [38, 39, 40, 41, 42, 51, 52, 43, 6, 53, 7, 8, 44, 46, 45, 9, 50, 48, 49].

Until now, numerical simulations have computed recoil velocities for non-spinning

unequal-mass black-hole binary systems [52, 43, 6] in the range $m_1 : m_2 = 1:1, \cdots, 4:1$ for spinning, non-precessing binary black holes [8, 7, 45], and also for precessing black holes with both equal [46, 44, 9], as well as, unequal masses [44]. Quite interestingly, there exist initial spin configurations for which the recoil velocity can be quite large, e.g., $\gtrsim 2500$ km/sec [44, 46, 7, 9], ejecting the final black hole from virtually any galactic potential. These large kicks can be produced in an equal-mass binary, having initial spins perpendicular to the orbital angular-momentum, opposite in directions and equal in magnitude. However, it is not yet clear whether those truly large recoil velocities are astrophysically likely [54, 55, 56, 57]. So far, due to limited computational resources, the numerical simulations have explored a rather small portion of the total parameter space. An analytical description of the recoil velocity can allow to explore quickly and efficiently a large portion of the parameter space, especially in presence of spins.

Analytical calculations, based on the post-Newtonian expansion or resummation of Einstein field equations [13, 21, 17, 19, 18, 36], have also made predictions for the recoil velocity [38, 39, 40, 41, 51]. Since the majority of the linear-momentum flux is emitted during the merger and ringdown phases, it is difficult to make definitive predictions for the recoil velocity using *only* analytical methods, unless they are calibrated to the numerical relativity results. In fact, as we shall see below, the final recoil velocity is determined by the contribution of several modes that add constructively or destructively during the transition plunge to merger to ringdown [8, 7, 50, 48, 49].

So far, in the non-spinning case, the adiabatic post-Newtonian formula of the linear-momentum flux computed at 2PN-order [41] has provided results consistent with numerical relativity all along the adiabatic inspiral until $\sim 50M$ before the peak of the waveform. Including for the first time the contribution from the ringdown phase, Ref. [51] predicted the final kick for non-spinning black holes employing the EOB model. Ref. [51] also pointed out that different post-Newtonian representation of the linear-momentum flux can lead to large uncertainties (by a factor ~ 4) in the prediction of the final recoil. By applying perturbative calculations which make use of the so-called close-limit approximation [14], and assuming for simplicity that the final black hole is a Schwarzschild black hole, Ref. [42] predicted the recoil for unequal-mass black holes moving on circular and eccentric orbits.

More recently, Ref. [53] provided the first estimates of the distribution of recoil velocities from spinning black-hole mergers using the EOB model [19, 18, 36] augmented with three QNMs [51, 10], and calibrated to the numerical relativity results. As a first-cut to the problem, Ref. [53] estimated the systematic errors on the recoil velocity due to this sub-optimal matching by varying the matching point between $r_{\rm match}/M = 2.5$–3.5 ($M\omega_{\rm match} = 0.1$–$0.2$). This range of variation corresponds to impose that the energy released beyond the matching point differs from some *fiducial value* [53] by $\sim 15\%$. Within these confidence limits, Ref. [53] found good agreement with previously reported results from numerical relativity. Using a Monte Carlo implementation of the EOB model [36], Ref. [53] was able to sample a large volume of black-hole parameter space and investigate the distribution of recoil velocities. For a range of mass ratios $1 \leq m_2/m_1 \leq 10$, spin magnitudes of $a_{1,2} = 0.9$, and uniform random spin orientations, Ref. [53] found that a fraction $f_{500} = 0.12^{+0.06}_{-0.05}$ of binaries have recoil velocities greater than 500 km/s and $f_{1000} = 0.027^{+0.021}_{-0.014}$ have kicks greater than 1000 km/s. These veloc-

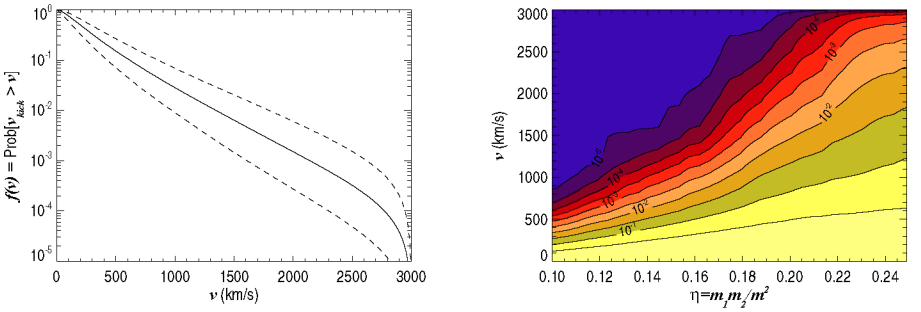

FIGURE 3. In the left panel we show the cumulative distribution function for kick velocities $v_{\rm kick} < v$ for equal masses $m_1 = m_2$ and random spins. The dashed lines represent 1-σ confidence level using the EOB model [36, 51, 10]. In the right panel we show the cumulative probability distribution as a function of symmetric mass ratio η. The contours of $f(v;\eta)$ represent the probability of having a recoil velocity greater than v. The spins have amplitude $a_1 = a_2 = 0.9$ and random orientation. (Both figures are adapted from Ref. [53].)

ities likely are capable of ejecting the final black hole from its host galaxy. Limiting the sample to comparable-mass binaries with $m_1/m_2 \lesssim 4$, the typical kicks are even larger, with $f_{500} = 0.36 \pm 0.13$ and $f_{1000} = 0.10^{+0.075}_{-0.052}$. In Fig. 3 we plot the cumulative distribution of recoil velocities, as obtained in Ref. [53].

The results of Ref. [53] were obtained assuming an initial random distribution of black-hole spins. What are the spin orientations in galactic mergers? In Ref. [55] the authors showed that when two black-hole accrete at least $\sim$ 1–10% of their masses during a gas rich galactic merger, torques from accreting gas will align the spins with the orbital angular momentum. However, without much gas the torque is inefficient, and the spin orientations can be generic. In fact, the post-Newtonian spin-precession equations [39] do not lead to any alignment of the spins with the orbital angular momentum, except for rather special cases [58] — for example for a nearly equal-mass binary with $m_1/m_2 \sim 1.22$, when the angle between one black-hole spin, say $\mathbf{S}_1$, and the orbital angular momentum is initially less than $\sim 10^{\rm o}$ or larger than $\sim 170^{\rm o}$, and the other spin $\mathbf{S}_2$ has a random orientation. In this case the spin $\mathbf{S}_2$ *locks* [58] to $\mathbf{S}_1$, and as the binary evolves toward merger the angle between the two spins tends to zero. Large mass-ratio binaries, e.g., $m_1/m_2 > 10^3$, can show a behaviour similar to the nearly equal-mass binary but only for cases when the initial angle between $\mathbf{S}_1$ and the orbital angular momentum is pretty close to zero or alternatively close to $180^{\rm o}$.

If large kicks (> 2500 km/sec) are likely, there might be a potential contradiction with observations of supermassive black holes residing in the centers of most galaxies in the local universe. An interesting explanation of how galaxies may retain their black holes, even if recoil velocities may be large, was proposed in Ref. [57]. The explanation is based on the simple observation that there are two competing effects that determine the fraction of galaxies today with a black hole. Large kicks can expel the black hole reducing the fraction of galaxies with black holes, but due to mergers the number of galaxies inevitably decreases, so the fraction with black holes can easily increase [57].

Taking into account these two competing effects, Ref. [57] estimated that even if we assume that the probability that a merging black hole is ejected due to gravitational recoil is one, the fraction of galaxies today retaining the central black hole is 50%. Including other astrophysical effects and making the merger-tree model more realistic, this percentage increases, becoming consistent to results from Ref. [54] which employed more sophisticated merger evolution codes.

Using several numerical relativity simulations of unequal masses and non-zero, non-precessing black hole spins, Ref. [50] made used of a multipolar analysis [59, 51] to shed light on how the recoil builds up throughout the inspiral, merger, and ringdown phases. Confirming previous results [7, 8] they found that multipole moments up to and including $\ell = 4$ are sufficient to accurately reproduce the final recoil velocity (within $\simeq 2\%$). They also found that only a few dominant modes contribute significantly to it (within $\simeq 5\%$). Introducing the linear-momentum flux vector

$$\mathbf{F} = \{F_x, F_y, F_z\}\,, \qquad \hat{\mathbf{F}} = \frac{\mathbf{F}}{|\mathbf{F}|}\,. \tag{1}$$

and limiting to spin non-precessing configurations for which the recoil velocity is directed in the orbital plane $x-y$, the linear-momentum flux is well approximated by the following pairs of modes [50]

$$\begin{aligned} F_x + iF_y &\simeq \frac{1}{672\pi}\left[-28i\,{}^{(3)}\mathrm{S}^{21}\,{}^{(3)}\mathrm{I}^{22*} - 2\sqrt{210}\,{}^{(3)}\mathrm{I}^{22}\,{}^{(4)}\mathrm{I}^{33*} - 14\sqrt{6}\,{}^{(4)}\mathrm{I}^{33}\,{}^{(5)}\mathrm{I}^{44*}\right], \\ &\equiv F^{21,22} + F^{22,33} + F^{33,44}\,, \qquad (2) \\ F_z &= 0\,, \qquad (3) \end{aligned}$$

where ${}^{(n)}\mathrm{I}^{\ell m}$ and ${}^{(n)}\mathrm{S}^{\ell m}$ are the n^{th} time derivatives of the radiative multipole moments [59, 50]. More specifically, I^{22}, I^{33}, I^{44} and S^{21}, are the (complex) mass-quadrupole, mass-octupole, mass-hexadecapole and current-quadrupole radiative moments, respectively. They can be expressed in terms of the source moments, i.e, in terms of the binary frequency, radial-separation and phase [59, 51, 50]. Furthermore, using $\mathbf{v} = \int \mathbf{F} dt$, we can write [50]

$$\frac{d}{dt}|\mathbf{v}| = \frac{d}{dt}(\hat{\mathbf{v}}\cdot\mathbf{v}) = \hat{\mathbf{v}}\cdot\mathbf{F}\,, \tag{4}$$

where $\hat{\mathbf{v}}\cdot\hat{\mathbf{v}} = 1$, and define [50]

$$\begin{aligned} v^{21,22} &= \int \hat{\mathbf{v}}\cdot\mathbf{F}^{21,22}\,dt\,, \qquad (5) \\ v^{22,33} &= \int \hat{\mathbf{v}}\cdot\mathbf{F}^{22,33}\,dt\,, \qquad (6) \\ v^{33,44} &= \int \hat{\mathbf{v}}\cdot\mathbf{F}^{33,44}\,dt\,, \qquad (7) \end{aligned}$$

which add linearly to give to total recoil velocity:

$$|\mathbf{v}| = v^{21,22} + v^{22,33} + v^{33,44}. \tag{8}$$

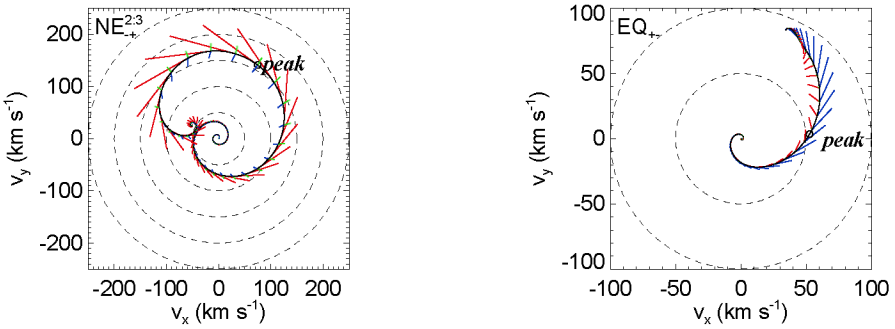

FIGURE 4. The recoil velocity vector evolving in the v_x–v_y plane (*black solid curve*), along with the flux vectors due to the three mode pairs at each time interval along the velocity trajectory. In the left (right) panel we show the data for the unequal-mass (equal-mass) case with spins aligned and anti-aligned with the angular momentum and magnitude ~ 0.2. These two cases are denoted as $\mathrm{NE}^{2:3}_{+-}$ and EQ_{+-}. The time t_{peak} is the time at which ${}^{(3)}I^{22}$ reaches its maximum. (Both figures are adapted from Ref. [50].)

As explained in Ref. [50], throughout the inspiral phase, the amplitude and rotational frequency of the flux vectors in Eq. (2) are monotonically increasing, giving the familiar outward-spiraling trajectory for the velocity vector. Then, in the ringdown phase, the dominant frequencies are nearly constant while the amplitudes decay exponentially for each mode, giving an inward-spiral that decays like a damped harmonic oscillator around the final asymptotic recoil velocity. These trajectories in velocity space, together with the instantaneous flux vectors from the competing mode-pairs in Eq. (2), can be seen in Fig. 4. The relative contributions to the total recoil velocity from the different multipole mode-pairs is instead shown in Fig. 5. Reference [50] found that even small changes in the mass ratios and spins orientations of the black holes can give a rather diverse selection of velocity trajectories. In the left (right) panels of Figs. 4, 5 we show the data for the unequal-mass (equal-mass) case with spins aligned and anti-aligned with the angular momentum and magnitude $\chi_{1,2} \sim 0.2$. These two cases are denoted as $\mathrm{NE}^{2:3}_{+-}$ and EQ_{+-}. Note in Fig. 5 the difference between the $\mathrm{NE}^{2:3}_{-+}$ run, dominated by the $F^{22,33}$ ($v^{22,33}$) flux (velocity) and a large anti-kick, and the EQ_{+-} run, which in contrast is dominated by the $F^{21,22}$ ($v^{21,22}$) flux (velocity) [50].

The absence of anti-kick in the EQ_{+-} run is consistent with the slowly rotating flux vector that does not spiral back inwards, as in the $\mathrm{NE}^{2:3}_{-+}$ run, but rather drifts off slowly towards infinity during the ringdown, as can be seen from Fig. 4. The difference between these two runs can be explained entirely by examining the real part of their fundamental QNM frequencies $\sigma_{\ell m 0}$ [50]. The latter determines the rotation rates of the flux vectors [50] during the ringdown: EQ_{+-} is dominated by $\omega_{220} - \omega_{210} = 0.08/M_{\mathrm{BH}}$, a much slower frequency than $\omega_{330} - \omega_{220} = 0.31/M_{\mathrm{BH}}$, which causes the rapid inward-spiral of the $\mathrm{NE}^{2:3}_{-+}$ run.

Using the multipolar analysis, Ref. [50] also tried to explain the remarkable difference between the amplitudes of planar and non-planar kicks for equal-mass spinning black

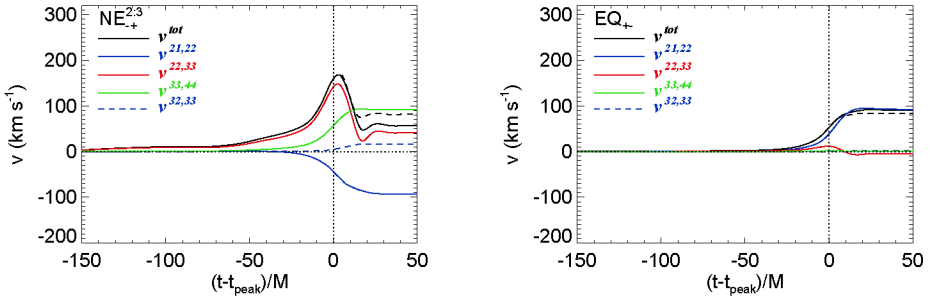

FIGURE 5. Relative contributions to the recoil velocity from the different multipole mode-pairs (2). ${}^{(3)}\mathrm{I}^{22}{}^{(4)}\mathrm{I}^{33*}$ (red curve) is the dominant mode for unequal-mass binary systems, while ${}^{(3)}\mathrm{S}^{21}{}^{(3)}\mathrm{I}^{22*}$ (blue curve) dominates for spinning, equal-mass binary systems. Also plotted is the contribution from the ${}^{(4)}\mathrm{S}^{32}{}^{(4)}\mathrm{I}^{33*}$ flux terms (blue dashed curve), demonstrating its very small contribution to the total recoil velocity. For $t > t_{\rm match} = t_{\rm peak}$, we include the quasi-analytical prediction for $v_{\rm RD}(t)$ (black dashed curves), based on the fundamental QNM. In the left (right) panel we show the data for the unequal-mass (equal-mass) case with spins aligned and anti-aligned with the angular momentum and magnitude $\chi_{1,2} \sim 0.2$. These two cases are denoted as $\mathrm{NE}^{2:3}_{+-}$ and EQ_{+-}. The time $t_{\rm peak}$ is the time at which ${}^{(3)}\mathrm{I}^{22}$ reaches its maximum. (Both figures are adapted from Ref. [50].)

holes, with spins on the orbital plane, opposite to each other and equal in magnitude. The planar configuration gives a kick of only ~ 500 km/sec in the case of maximal spin [8, 7, 45, 49], whereas the non-planar configuration of ~ 3000km/sec. The non-planar configuration exhibits π-symmetry, i.e., it is invariant under a rotation by an angle π about the axis perpendicular to the orbital plane. Thus, linear momentum can be radiated only along the direction perpendicular to the orbital plane. Furthermore, as observed in Refs. [48, 50] the kick is produced by the imbalance between the $l = 2$, $m = 2$ and $l = 2$, $m = -2$ modes, i.e., is due to the difference in energy radiated toward the north and south hemispheres [48].

ACKNOWLEDGMENTS

The author wishes to thank Greg Cook, Yi Pan, Frans Pretorius, Jeremy Schnittman, and the Goddard-NASA group, John Baker, Williams Boggs, John Centrella, Bernard Kelly, Sean McWilliams, Jim van Meter, for the fruitful collaborations reviewed in this Proceedings.

The author acknowledges support from NSF grant PHY-0603762 and from the Alfred P. Sloan Foundation.

REFERENCES

1. F. Pretorius, *Phys. Rev. Lett.* **95**, 121101 (2005).
2. M. Campanelli, C.O. Lousto, P. Marronetti, and Y. Zlochower, *Phys. Rev. Lett.* **96**, 111101 (2006).

3. J. Baker, J. Centrella, D. Choi, M. Koppitz, and J. van Meter, *Phys. Rev. Lett.* **96**, 111102 (2006).
4. U. Sperhake, gr-qc/0606079.
5. B. Szilagyi, D. Pollney, L. Rezzolla, J. Thornburg, and J. Winicour, *Class. Quant. Grav.* **24**, S275 (2007).
6. J.A. Gonzalez, U. Sperhake, B. Brügmann, M. Hannam, and S. Husa, *Phys. Rev. Lett.* **98**, 091101 (2007).
7. F. Herrmann, I. Hinder, D. Shoemaker, P. Laguna, and R.A. Matzner, gr-qc/0701143.
8. M. Koppitz, D. Pollney, C. Reisswig, L. Rezzolla, J. Thornburg, P. Diener, and E. Schnetter, gr-qc/0701163.
9. W. Tichy and P. Marronetti, gr-qc/0703075.
10. A. Buonanno, G. Cook, and F. Pretorius, *Phys. Rev. D* **75**, 124018 (2007).
11. A. Buonanno, Y. Pan, J.G. Baker, J. Centrella, B.J. Kelly, S.T. McWilliams, and J.R. van Meter, in press on *Phys. Rev. D* arXiv:0706.3732 [gr-qc].
12. T. Damour and A. Nagar, gr-qc/07052519.
13. See, e.g., L. Blanchet, *Living Rev. Rel.* **5**, 3 (2002).
14. R.H. Price and J. Pullin, *Phys. Rev. Lett.* **72**, 3297 (1994); R.J. Gleiser, C.O. Nicasio, R. Price, and J. Pullin, *Class. Quant. Grav.* **13**, L117 (1996); *Phys. Rev. Lett.* **77**, 4483 (1996); P. Anninos, D. Hobill, E. Seidel, L. Smarr, and W.M. Suen, *Phys. Rev. Lett.* **71**, 2851 (1993); Z. Andrade and R. H. Price, *Phys. Rev. D* **56**, 6336 (1997); J. Baker, A. Abrahams, P. Anninos, S. Brandt, R. Price, J. Pullin, and E. Seidel, *Phys. Rev. D* **55**, 829 (1997).
15. W. Press, *Astrophys. J. Letters* **170**, L105 (1971); C.J. Goebel, *Astrophys. J. Letters* **172**, L95 (1972).
16. M. Davis, R. Ruffini, W.H. Press, and R.H. Price, *Phys. Rev. Lett.* **27**, 1466 (1971); M. Davis, R. Ruffini, and J. Tiomno, *Phys. Rev. D* **5**, 2932 (1972).
17. A. Buonanno, and T. Damour, *Phys. Rev. D* **59**, 084006 (1999).
18. T. Damour, P. Jaranowski, and G. Schäfer, *Phys. Rev. D* **62**, 084011 (2000).
19. A. Buonanno, and T. Damour, *Phys. Rev. D* **62**, 064015 (2000).
20. A. Buonanno, and T. Damour, *Proceedings of the Ninth Marcel Grossmann Meeting* (Rome, July 2000) gr-qc/0011052.
21. T. Damour, B.R. Iyer, and B.S. Sathyaprakash, *Phys. Rev. D* **57**, 885 (1998).
22. J. Baker, B. Brügmann, M. Campanelli, C.O. Lousto and R. Takahashi, *Phys. Rev. Lett.* **87**, 121103 (2001).
23. J. D. Bekenstein, *Astrophys. J.* **183**, 657 (1973).
24. F. I. Cooperstock, *Astrophys. J.* **213**, 250 (1977).
25. M.J. Fitchett, *Mon. Not. R. Astr. Soc.* **203**, 1049 (1983); M. J. Fitchett and S. Detweiler, *Mon. Not. R. Astr. Soc.* **211**, 933 (1984).
26. M.G. Haehnelt, *Mon. Not. R. Astr. Soc.* **269**, 199 (1994); K. Menou, Z. Haiman, and V.K. Narayanan, *Astrophys. J.* **558**, 535 (2001); M. Volonteri, F. Haardt, and P. Madau, *Astrophys. J.* **582**, 559 (2003).
27. D. Merritt, M. Milosavljevic, M. Favata, and S.A. Hughes, *Astrophys. J.* **607**, L9 (2004).
28. A. Abramovici et al., *Science* **256**, 325 (1992); http://www.ligo.caltech.edu.
29. B. Caron et al., *Class. Quant. Grav.* **14**, 1461 (1997); http://www.virgo.infn.it.
30. H. Lück et al., *Class. Quant. Grav.* **14**, 1471 (1997); http://www.geo600.uni-hannover.de.
31. M. Ando et al., *Phys. Rev. Lett.* **86**, 3950 (2001); http://tamago.mtk.nao.ac.jp.
32. http://www.lisa-science.org/resources/talks-articles/science/lisa_science_case.pdf
33. L.S. Finn, *Phys. Rev. D* **46**, 5236 (1992); L. S. Finn and D.F. Chernoff, *Phys. Rev. D* **47**, 2198 (1993).
34. C.V. Vishveshwara, *Nature* **227**, 936 (1970); B. Schutz and C.M. Will, *Astrophys. J.* **291**, 33 (1985); S. Chandrasekhar and S. Detweiler, *Proc. R. Soc. Lond. A* **344**, (1975) 441; E. W. Leaver, *Proc. R. Soc. Lond. A* **402**, (1985) 285.
35. T. Damour, *Phys. Rev. D* **64**, 124013 (2001).
36. A. Buonanno, Y. Chen, and T. Damour, *Phys. Rev. D* **74**, 104005 (2006).
37. T. Damour and A. Nagar, gr-qc/07043550.
38. A. Wiseman, *Phys. Rev. D* **46**, 1517 (1992).
39. L. Kidder, *Phys. Rev. D* **52**, 821 (1995).

40. M. Favata, S.A. Hughes, and D. Holz, *Astrophys. J.* **607**, L5 (2004).
41. L. Blanchet, M.S.S. Qusailah, and C.M. Will, *Astrophys. J.* **635**, 508 (2006).
42. C.F. Sopuerta, N. Yunes, and P. Laguna, *Phys. Rev. D* **74**, 124010 (2006); Erratum-ibid.D **75**, 069903 (2007); C.F. Sopuerta, N. Yunes, and P. Laguna, *Astrophys. J.* **656**, L9 (2007).
43. J.G. Baker, J. Centrella, D. Choi, M. Koppitz, J. R. van Meter, and M.C Miller, *Astrophys. J.* **653**, L93 (2006).
44. M. Campanelli, C.O. Lousto, Y. Zlochower, and D. Merritt, *Astrophys. J.* **659**, L5 (2007); M. Campanelli, C.O. Lousto, Y. Zlochower, and D. Merritt, *Phys. Rev. Lett.* **98**, 231102 (2007).
45. J.G. Baker, W.D. Boggs, J. Centrella, B.J. Kelly, S.T. McWilliams, M. C. Miller, and J.R. van Meter, `astro-ph/0702390`.
46. J.A. Gonzalez, M.D. Hannam, U. Sperhake, B. Brugmann, and S. Husa, *Phys. Rev. Lett.* **98**, 231101 (2007).
47. F. Herrmann, I. Hinder, D. Shoemaker, P. Laguna, and R.A. Matzner `arXiv:0706.2541` [gr-qc].
48. B. Brügmann, J.A. Gonzales, M. Hannam, S. Husa, and U. Sperhake, `arXiv:0703.0135` [gr-qc].
49. D. Pollney et al., `arXiv:0703.2559` [gr-qc].
50. J. Schnittman, A. Buonanno, J. R. van Meter, J.G. Baker, W.D. Boggs, J. Centrella, B.J. Kelly, and S.T. McWilliams, submitted to *Phys. Rev. D* `ArXiv:0707.0301` [astro-ph].
51. T. Damour and A. Gopakumar, *Phys. Rev. D* **73**, 124006 (2006).
52. F. Herrmann, D. Shoemaker, and P. Laguna, `gr-qc/0601026`.
53. J. Schnittman and A. Buonanno, *Astrophys. J.* **662**, L63 (2007).
54. M. Volonteri, *Astrophys. J.* **663**, L5 (2007).
55. T. Bogdanovic, C.S. Reynolds, and M.C. Miller, *Astrophys. J.* **661**, L147 (2007).
56. A. Loeb, `astro-ph/0703722`.
57. J. Schnittman, `arXiv:0706.1548` [astro-ph].
58. J. Schnittman, *Phys. Rev. D* **70**, 124020 (2004).
59. K.S. Thorne, *Rev. Mod. Phys.* **52**, 299 (1980); L. Blanchet and T. Damour, *Ann. Inst. H. Poincaré* **50**, 377 (1989); L. Blanchet and G. Schäfer, *Mon. Not. R. Astr. Soc.* **239**, 845 (1989); L. Blanchet, T. Damour, and G. Schäfer, *Mon. Not. R. Astr. Soc.* **242**, 289 (1990); W. Junker and G. Schäfer, *Mon. Not. R. Astr. Soc.* **254**, 146 (1992).